The 8th European Congress on Computational Methods in Applied Sciences and Engineering
ECCOMAS Congress 2022
5-–9 June 2022, Oslo, Norway

INVESTIGATION OF THE PANS METHOD FOR THE PREDICTION OF AERODYNAMIC NOISE AROUND A CIRCULAR CYLINDER

AREZOO MOOSAVIFARD [1,2], ELENA KOLB [2], MICHAEL SCHÄFER [1,2] AND SUAD JAKIRLIC [1,3]

[1] Computational Engineering Graduate School ,
Technical University of Darmstadt,
Dolivostr. 15, Darmstadt 64293, Hessen, Germany,
e-mail: moosavifard@gsc.tu-darmstadt.de

[2] Institute of Numerical Methods in Mechanical Engineering,
Technical University of Darmstadt,
Dolivostr. 15, Darmstadt 64293, Hessen, Germany,

[3] Institute of Fluid Mechanics and Aerodynamics,
Technical University of Darmstadt,
Alarich-Weiss-Str. 10, Darmstadt 64287, Hessen, Germany

Key words: Partially-Averaged Navier–Stokes, Scale-supplying variable, Computational aeroacoustics, Splitting approach, Circular cylinder.

Abstract.

Aeroacoustics is the field of studying flow-induced sound, which results from the interaction of unsteady flow with solid structures, such as aircraft and automobiles. Different methods are available to achieve this, including theoretical, experimental, and computational methods. Due to the high costs of experiments, the concentration on computational methods has increased. Computational aeroacoustics (CAA), based on computational fluid dynamics (CFD), has received special attention from researchers because of its outstanding capability to get acceptable results with reasonable computational costs. The partially-Averaged Navier Stokes (PANS) method is a hybrid LES/RANS method based on dynamic resolution parameters. The SSV-PANS method is a $k-\epsilon-\zeta-f$ based PANS method with an additional modeled equation for the resolved kinetic energy. This method has been implemented in FASTEST, an in-house finite-volume solver to compute the flows in complex applications. This study aims to investigate the aeroacoustic performance of the SSV-PANS method compared to a reference Large-eddy Simulation [1] regarding the computational accuracy and costs. To do this, hybrid method based on decomposing the fluid variables into incompressible hydrodynamics and compressible perturbation equations is used to study the aerodynamic noise. The aeroacoustic sources are computed from the incompressible flow field using the SSV-PANS method. In addition, the Kirchhoff wave extrapolation method is used to have an efficient evaluation of the far-field noise.

1 Introduction

The research field of aeroacoustics studies flow-induced sound resulting from the interaction of unsteady flow with solid structures to understand the sound generating mechanisms. It has an undeniable role in designing bridges, buildings, vehicles, aircraft, and other structures. Different methods are available to achieve this goal, including experimental and computational methods. However, due to the high costs of experiments, the concentration on computational methods has increased. The research field of CAA was started with the work of Lighthill [2] in the 1950s, which rearranges the compressible Navier-Stokes equations into the form of the inhomogeneous wave equation. In order to get an accurate insight into the turbulent flow noise, getting the most accurate aerodynamic sources with the available computational resources is of great importance. Hybrid methods for predicting the noise at low Mach numbers are common numerical methods that mostly decompose fluid variables into incompressible and perturbed compressible variables. The main goal of this research is to study the performance of the SSV-PANS method in resolving turbulent sound sources. To do this, a technique using a splitting approach based on the formulation given by Kornhaas et al. [3], which was initially introduced by Hardin and Pope [4] is used. The method is based on decomposing the fluid variables into incompressible flow and compressible perturbation equations. Therefore, the aeroacoustic sources are computed from the incompressible flow field. The Reynolds Averaged Navier-Stokes equations (RANS) method [5], which is widely used in industry, is not accurate enough for CAA problems. On the other hand, Large-eddy simulation (LES) [6] with its accurate results and high computational cost, is hard to use for industrial purposes. Besides the pure LES and RANS methods, the hybrid RANS/LES methods use LES when there is a need for more resolved turbulence features, and use RANS when modeling all the turbulence gives adequate results. With hybrid methods, the computational cost is less than LES, while the accuracy is better than RANS. Among the hybrid LES/RANS methods, the Partially-Averaged Navier Stokes (PANS) method has shown its capability to give promising results over the years. Girimaji ([7], [8]) developed the PANS method as a continuous approach for hybrid RANS/LES methods with seamless coupling between the RANS and LES regions. This method can smoothly bridge from RANS to DNS with two resolution parameters:

- The unresolved-to-total ratios of kinetic energy (f_k)
- The unresolved-to-total ratio of dissipation (f_ϵ).

The PANS decomposition of the velocity field is based on the kinetic energy content rather than the cut-off wavenumber, which means the model is designed to apply a proper balance between the resolved and modeled kinetic energy [7]. In the original formulation of PANS, Girimaji used a constant value for the resolution parameters for conducting all the following calculations [7]. Later, a two-stage PANS method where the f_k is specified by a one-time RANS calculation and kept constant in time was proposed by Girimaji, and Abdol-Hamid [9]. However, they also mentioned that this method could cause inaccurate distribution of f_k due to the inaccurate RANS calculation. So it is more reasonable for the f_k value to be modified spatially and temporally, which was first done by Huan et al. [10]. In 2011 an improved PANS method using the $k-\epsilon-\zeta-f$ turbulence model was used to improve the near-wall behavior. The original model ([7]) was extended with an additional transport equation for the velocity scale

ratio ζ and an equation for the elliptic relaxation function f [11]. The scale-supplying variable (SSV) method [12], which is used in this research, is a recent approach for the PANS model, which shows excellent accuracy while having acceptable computational cost. This method solves an additional modeled equation for the resolved kinetic energy to supply the information for the correct cut-off scale and continuously updates the resolution parameter f_k and is dynamically specified in time and space depending on the flow and the available grid. Using the SSV-equation, there is no need for the expensive spatial (or temporal) averaging process.

The method has been implemented in FASTEST [13], which is an in-house finite-volume solver for the computation of flows in complex applications. To compute the sound pressure level (SPL) in the far-field more efficiently, a correction method developed by Seo and Moon [14] for the finite span and a convected Kirchhoff wave extrapolation method [15] are used. In section 2, the computational methodology and the numerical schemes are explained. First, the governing equations describing the SSV-PANS method and then the acoustic equations are presented used for the prediction of the far-field SPL. In section 3, first, the method is validated using the periodic 2D hill test case. Second, the cylinder's hydrodynamic field is studied. Finally, the aeroacoustic results of the method are presented and compared with reference data.

2 Computational methodologies

In the current research, the acoustic/viscous splitting technique in the formulation provided by Kornhaas et al. [3] is used, which is valid for flows with low Mach numbers ($Ma < 0.3$). The flow field includes the incompressible flow field and acoustic fluctuations. First, the SSV-PANS method for the computation of incompressible hydrodynamic and then the acoustic method are explained.

2.1 Partially-Averaged Navier–Stokes (PANS)

The Partially-Averaged Navier–Stokes (PANS) equations are written in terms of filtered velocity and pressure fields [16], as follows:

$$\frac{\partial U_\mathrm{i}}{\partial t} + U_\mathrm{j}\frac{\partial U_\mathrm{i}}{\partial x_\mathrm{j}} + \frac{\partial \tau(V_\mathrm{i}, V_\mathrm{j})}{\partial x_\mathrm{j}} = -\frac{1}{\rho}\frac{\partial p}{\partial x_\mathrm{j}} + \nu\frac{\partial^2 U_\mathrm{i}}{\partial x_\mathrm{j}\partial x_\mathrm{j}}, \tag{1}$$

where p is the filtered pressure field and V_i is the instantaneous velocity which is decomposed to partially filtered and sub-filter components as:

$$V_\mathrm{i} = U_\mathrm{i} + u_\mathrm{i}. \tag{2}$$

Using the Boussinesq approximation the sub-filter stress reads:

$$\tau(V_\mathrm{i}, V_\mathrm{j}) = -2\nu_\mathrm{u} S_\mathrm{ij} + 2/3 k_\mathrm{u}\delta_\mathrm{ij}, \tag{3}$$

where k_u is the unresolved kinetic energy. The unresolved eddy viscosity ν_u and the resolved stress tensor S_ij are given as:

$$\nu_\mathrm{u} = c_\mu\frac{k_u^2}{\epsilon_\mathrm{u}} \quad \text{and} \quad S_\mathrm{ij} = 1/2\left(\frac{\partial U_\mathrm{i}}{\partial x_\mathrm{j}} + \frac{\partial U_\mathrm{j}}{\partial x_\mathrm{i}}\right), \tag{4}$$

where ϵ_u is the unresolved dissipation. The final set of equations for k_u and ϵ_u are [8]:

$$\frac{\partial k_\mathrm{u}}{\partial t} + U_\mathrm{j}\frac{\partial k_\mathrm{u}}{\partial x_\mathrm{j}} = P_\mathrm{u} - \epsilon_\mathrm{u} + \frac{\partial}{\partial x_\mathrm{j}}\left(\frac{\nu_\mathrm{u}}{\sigma_\mathrm{ku}}\frac{\partial k_\mathrm{u}}{\partial x_\mathrm{j}}\right), \tag{5}$$

$$\frac{\partial \epsilon_\mathrm{u}}{\partial t} + U_\mathrm{j}\frac{\partial \epsilon_\mathrm{u}}{\partial x_\mathrm{j}} = C_{\epsilon 1}P_\mathrm{u}\frac{\epsilon_\mathrm{u}}{k_u} - C^*_{\epsilon 2}\frac{\epsilon_\mathrm{u}^2}{k_u} + \frac{\partial}{\partial x_\mathrm{j}}\left(\frac{\nu_\mathrm{u}}{\sigma_{\epsilon\mathrm{u}}}\frac{\partial \epsilon_\mathrm{u}}{\partial x_\mathrm{j}}\right) \tag{6}$$

with the model coefficients defined as:

$$C^*_{\epsilon 2} = C_{\epsilon 1} + \frac{f_\mathrm{k}}{f_\epsilon}(C_{\epsilon 2} - C_{\epsilon 1}), \qquad \sigma_{k_\mathrm{u}} = \sigma_k\frac{f_\mathrm{k}^2}{f_\epsilon}, \qquad \sigma_{\epsilon_u} = \sigma_\epsilon\frac{f_\mathrm{k}^2}{f_\epsilon}. \tag{7}$$

The resolution parameter for the unresolved-to-total ratios of kinetic energy and for the unresolved-to-total ratios of dissipation are :

$$f_\mathrm{k} = \frac{k_\mathrm{u}}{k}, \qquad f_\epsilon = \frac{\epsilon_u}{\epsilon}. \tag{8}$$

These resolution parameters can take values between zero and one to achieve different resolution ratios. Following Girimaji and Abdul-Hamid [7], f_k is calculated using Equation 8 with a minimum value of:

$$f_\mathrm{k} \geq \frac{1}{\sqrt{C_\mu}}\left(\frac{\Delta}{\Lambda}\right)^{2/3}, \qquad \Lambda = \frac{k^{3/2}}{\epsilon}, \qquad \Delta = (\Delta_\mathrm{x}\Delta_\mathrm{y}\Delta_\mathrm{z})^{1/3}, \tag{9}$$

where Δ is the grid cells dimension and Λ the integral length scale of turbulence. The parameter f_ϵ is set to 1, which is valid for high Reynolds number flows [12]. The four-equation PANS model based on the $k-\epsilon-\zeta-f$ RANS model was developed by Basara et al. [11], which is called PANS $k-\epsilon-\zeta-f$ method. This model is derived from the ν^2-f model [17], which improves the near-wall behavior prediction. A transport equation for the wall-normal velocity scale ratio ζ_u $\left(=\overline{\nu_\mathrm{u}^2}/k_\mathrm{u}\right)$ is solved instead of one for the velocity scale ν_u^2. The final set of $k-\epsilon-\zeta-f$ PANS model equations are briefly presented below:

$$\frac{\partial k_\mathrm{u}}{\partial t} + U_\mathrm{j}\frac{\partial k_\mathrm{u}}{\partial x_\mathrm{j}} = P_\mathrm{u} - \epsilon_\mathrm{u} + \frac{\partial}{\partial x_\mathrm{j}}\left[\left(\nu + \frac{\nu_\mathrm{u}}{\sigma_\mathrm{ku}}\right)\frac{\partial k_\mathrm{u}}{\partial x_\mathrm{j}}\right], \tag{10}$$

$$\frac{\partial \epsilon_\mathrm{u}}{\partial t} + U_\mathrm{j}\frac{\partial \epsilon_\mathrm{u}}{\partial x_\mathrm{j}} = C_{\epsilon 1}P_\mathrm{u}\frac{\epsilon_\mathrm{u}}{k_u} - C^*_{\epsilon 2}\frac{\epsilon_\mathrm{u}^2}{k_u} + \frac{\partial}{\partial x_\mathrm{j}}\left[\left(\nu + \frac{\nu_\mathrm{u}}{\sigma_{\epsilon\mathrm{u}}}\right)\frac{\partial \epsilon_\mathrm{u}}{\partial x_\mathrm{j}}\right], \tag{11}$$

$$\frac{\partial \zeta_\mathrm{u}}{\partial t} + U_\mathrm{j}\frac{\partial \zeta_\mathrm{u}}{\partial x_\mathrm{j}} = f_\mathrm{u} - \frac{\zeta_\mathrm{u}}{k_\mathrm{u}}P_\mathrm{u} - \frac{\zeta_\mathrm{u}}{k_\mathrm{u}}\epsilon_\mathrm{u}(1-f_\mathrm{k}) + \frac{\partial}{\partial x_\mathrm{j}}\left[\left(\nu + \frac{\nu_\mathrm{u}}{\sigma_{\zeta\mathrm{u}}}\right)\frac{\partial \zeta_\mathrm{u}}{\partial x_\mathrm{j}}\right], \tag{12}$$

$$L_\mathrm{u}^2\bigtriangledown^2 f_\mathrm{u} - f_\mathrm{u} = \frac{1}{T_\mathrm{u}}\left(c_1 + c_2\frac{P_\mathrm{u}}{\epsilon_\mathrm{u}}\right)(\zeta_\mathrm{u} - \frac{2}{3}), \tag{13}$$

with $\nu_\mathrm{u} = C_\mu\zeta_u k_\mathrm{u}^2/\epsilon_\mathrm{u}$. The constants C_μ, c_1, c_2, $C_{\epsilon 2}$ are equal to 0.22, 0.4, 0.65 and 1.9 , respectively. The length scale L_u and the time scale T_u are as following:

$$T_\mathrm{u} = \max\left[\frac{k_\mathrm{u}}{\epsilon}, C_\tau\left(\frac{\nu}{\epsilon}\right)^{1/2}\right], \qquad L_\mathrm{u} = C_\mathrm{L}\max\left[\frac{k_\mathrm{u}^{3/2}}{\epsilon}, C_\eta\left(\frac{\nu^3}{\epsilon}\right)^{1/4}\right]. \tag{14}$$

As mentioned earlier, Basara and Girimaji [18] proposed a new equation called the integral scale supplying variable equation to solve the resolved kinetic energy. Before that, the resolved turbulence was calculated from differences between the instantaneous filtered velocity and the averaged velocity field to have the integral scale of turbulence, which was computationally expensive and was replaced by the SSV equation. In this method the total kinetic energy is decomposed into unresolved kinetic energy and the scale-supplying resolved kinetic energy:

$$k = k_{\mathrm{ssv}} + k_{\mathrm{u}}. \tag{15}$$

Then, by using the PANS basic principles and following the similar procedure of the unresolved kinetic energy, the final form of the k_{ssv} equation becomes:

$$\frac{\partial k_{\mathrm{ssv}}}{\partial t} + U_{\mathrm{j}}\frac{\partial k_{\mathrm{ssv}}}{\partial x_{\mathrm{j}}} = (1 - f_{\mathrm{k}})(P - \epsilon) + \frac{\partial}{\partial x_{\mathrm{j}}}\left[\left(\nu + \frac{\nu_{\mathrm{u}}}{\sigma_{\mathrm{ku}}}\right)\frac{\partial k_{\mathrm{ssv}}}{\partial x_{\mathrm{j}}}\right]. \tag{16}$$

The complete derivation of the scale-supplying resolved kinetic energy k_{ssv} equation as well as the preliminary results for a turbulent channel flow is presented in [18] and the results for a square cylinder is presented in the work of Basara et al. in [12]. After solving Equation 16 , the total kinetic energy is again calculated using Equation 15 and the f_k is again calculated using Equation 9. The new SSV-PANS based on the $k - \epsilon - \zeta - f$ model is validated for a periodic 2D-hill presented in section 3. It is then used to study the aeroacoustic results of the turbulent flow around a circular cylinder.

2.2 Aeroacoustics

The flow quantities are decomposed into an incompressible flow field and an acoustic field:

$$\rho = \rho^{\mathrm{ic}} + \rho^{\mathrm{a}}, \qquad \nu_{\mathrm{i}} = \nu_{\mathrm{i}}^{\mathrm{ic}} + \nu_{\mathrm{i}}^{\mathrm{a}}, \qquad p = p^{\mathrm{ic}} + p^{\mathrm{a}}, \tag{17}$$

where *ic* stands for incompressible and *a* for acoustic quantities. The acoustic equations can be obtained by inserting the above equations into compressible conservation equations for mass and momentum. For low Mach number flows, and by neglecting the higher-order acoustic terms, the final form of the Linearized Euler equations (LEE) can be accomplished as [3]:

$$\frac{\partial \rho^{\mathrm{a}}}{\partial t} + \rho^{\mathrm{ic}}\frac{\partial \nu_{\mathrm{i}}^{\mathrm{a}}}{\partial x_{\mathrm{i}}} + \nu_{\mathrm{i}}^{\mathrm{ic}}\frac{\partial \rho^{\mathrm{a}}}{\partial x_{\mathrm{i}}} = 0, \tag{18}$$

$$\rho^{\mathrm{ic}}\frac{\partial \nu_{\mathrm{i}}^{\mathrm{a}}}{\partial t} + \rho^{\mathrm{ic}}\nu_{\mathrm{j}}^{\mathrm{ic}}\frac{\partial \nu_{\mathrm{i}}^{\mathrm{a}}}{\partial x_{\mathrm{j}}} + \frac{\partial p^{\mathrm{a}}}{\partial x_{\mathrm{i}}} = 0, \tag{19}$$

$$\frac{\partial p^{\mathrm{a}}}{\partial t} + C_{\infty}^{2}\rho^{\mathrm{ic}}\frac{\partial \nu_{\mathrm{i}}^{\mathrm{a}}}{\partial x_{\mathrm{i}}}\partial x_{\mathrm{i}} + \nu_{\mathrm{i}}^{\mathrm{ic}}\frac{\partial p^{\mathrm{a}}}{\partial x_{\mathrm{i}}} = -\frac{\partial p^{\mathrm{ic}}}{\partial t}, \tag{20}$$

which are the governing equations for acoustic density, ρ_a, acoustic velocity, u_a, and acoustic pressure, p_a, respectively. C_∞ $\left(= \sqrt{(\partial p/\partial \rho)_S}\right)$ is the speed of sound. The left-hand side of the Equations 18 to 20 represent the effects of acoustic wave propagation, while the right-hand side contains the acoustic source term computed from the incompressible flow solution.

2.3 Long-span bodies method

Since using the periodic boundary condition for LEE equations (Equation 18 to Equation 20), can cause nonphysically correlated acoustic forcing when the same span length as the turbulent length scale is used, a computationally more efficient approach [14] is used here. A two-dimensional acoustic field (at the zero span-wise wave length) is calculated at the mid-span plane with acoustic sources and hydrodynamic variables integrated in the span-wise direction:

$$\tilde{q}(x_1, x_2, t) = \int_{-\mathrm{L_s}/2}^{\mathrm{L_s}/2} q(x_1, x_2, x_3, t) dx_3, \tag{21}$$

where L_s is the span length used for the hydrodynamic field. The computed far-field acoustic pressure is then corrected by Equation 22. Considering the Fourier-transformed wave equation in the span-wise direction, the three-dimensional radiated far-field acoustic pressure in the frequency domain. p^{a} is related to the two-dimensional predicted acoustic pressure $\tilde{p}^{\mathrm{a}}$:

$$p^{\mathrm{a}}(x_1, x_2, 0, \omega) \approx \tilde{p}^{\mathrm{a}}(x_1, x_2, \omega) \frac{1+i}{2} \sqrt{\frac{\omega}{C_\infty \pi r}}, \tag{22}$$

where ω is the angular frequency and r $\left(= \sqrt{x_1^2 + x_2^2}\right)$ is the observer's distance. A complete derivation of this relationship which is proposed by Oberai et al., is presented in [19].

2.4 Far-field acoustics

At low Mach numbers, generated acoustic waves have a range of wavelengths, which can be resolved when grids are fine enough to the far-field boundary. When an observer's position is far from the noise source, the acoustic domain can be truncated, and the acoustic pressure calculated from the LEE method can be extrapolated from the Kirchhoff surface, which encloses all sound sources to the observer's position using the 2D Kirchhoff method [15]:

$$\begin{aligned} \tilde{p}^{\mathrm{a}}(x_1, x_2, \omega) = \frac{j\beta}{4} \int_{\mathrm{S_k}} \Bigg\{ & \frac{\partial \tilde{p}^{\mathrm{a}}}{\partial y_i} H_0^{(2)}\left(\frac{k}{\beta^2} r_\beta\right) + \frac{k\tilde{p}^{\mathrm{a}}}{\beta^2} \Bigg[\frac{\partial r_\beta}{\partial y_i} H_1^{(2)}\left(\frac{k}{\beta^2} r_\beta\right) \\ & - j\mathrm{M} \frac{\partial y_1}{\partial y_i} H_0^{(2)}\left(\frac{k}{\beta^2} r_\beta\right) \Bigg] \times e^{j\frac{\mathrm{M}k r_1}{\beta^2}} (n_i - \mathrm{M}^2 n_1) \Bigg\} dS_k, \end{aligned} \tag{23}$$

where $\mathrm{M} = U_\infty / C_\infty$. n_{i} is the i-th component of the outward pointing unit normal vector on the Kirchhoff surface. r_β $(= \sqrt{(x_1 - y_1)^2 + \beta^2 (x_2 - y_2)^2})$ is the distance from source to observer's position with the Prandtl-Glauert factor β $(= \sqrt{1 - \mathrm{M}^2})$. Furthermore, k $(= \omega / \mathrm{c}_\infty)$ is the wave number and $j = \sqrt{-1}$. The Hankel function of order j and second kind is given by H_j^2. The derivation of Equation 23 is presented in the work of Gloerfelt et al. [15]. The sound pressure level (SPL) at the far-field with the simulated span L_s can be estimated with the aforementioned method. To get the SPL for the required span, L, a correction is needed. Therefore, a correction method used by Seo and Moon[14] is applied here:

$$SPL = SPL_s + SPL_c, \tag{24}$$

$$SPL_c = \begin{cases} 10\log(N) & \text{if} \quad L_c^a/L_s \leq 1/\sqrt{\pi} \\ 10\log(L_c^a/L_s) + 10\log(\sqrt{\pi}N) & \text{if} \quad 1/\sqrt{\pi} < L_c^a/L_s < N/\sqrt{\pi} \\ 20\log(N) & \text{if} \quad L_c^a/L_s \geq N/\sqrt{\pi} \end{cases} \tag{25}$$

where N $(=L/L_s)$ is the ratio of the required span length to the simulated span length.

3 Results

3.1 Flow over two-dimensional periodic hill

The periodic 2D hill test case is simulated to validate the SSV-PANS model's implementation in the FASTEST flow solver. The computational domain consists of a channel with a length of $L_x = 9h$, the height of $L_y = 3.035h$, and a span-wise length of $L_z = 4.5h$, with h being the hill's height. The top and the bottom edges are considered to have no-slip wall boundary conditions. In the stream-wise and span-wise directions, a periodic boundary is applied. The computational domain consists of 0.7×10^6 control volumes (CVs). The simulation is evaluated over 50 flow-through cycles. The results are compared with the reference LES results [20] with 4.6×10^6 CVs. The Reynolds number based on the bulk velocity $\left(Re_\mathrm{b} = u_b h/\nu \right)$ is 10595. Setting a pressure gradient acting on the flow is necessary to achieve the desired bulk velocity. The averaged stream-wise velocity contour and streamlines of the flow are shown in Figure 1. The

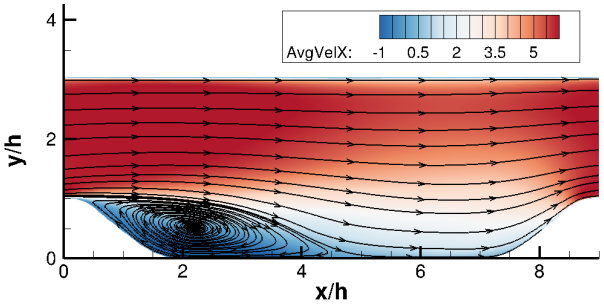

Figure 1: Streamlines in periodic 2D hill flow obtained by SSV-PANS

streamlines show a re-circulation region separated from the mainstream at the inflow and a reattachment in the middle of the bottom wall. To compare the SSV-PANS results with LES results [20], the distribution of the skin friction coefficient, $C_f = \tau_w/\frac{1}{2}\rho U_0^2$, along the bottom wall is shown in Figure 2 and the separation and reattachment point locations are presented in Table 1. It can be concluded that the results of the SSV-PANS model agree well with the reference data.

3.2 Flow over the circular cylinder

The main objective of this paper is to study the aeroacoustic performance of the SSV-PANS method in comparison with LES. For this purpose, the flow past a circular cylinder and the acoustic quantities generated by the turbulent flow are investigated. The Reynolds number based on the cylinder diameter ($D = 0.01$ m) is Re $= 48,000$ and the Mach number is Ma $=$

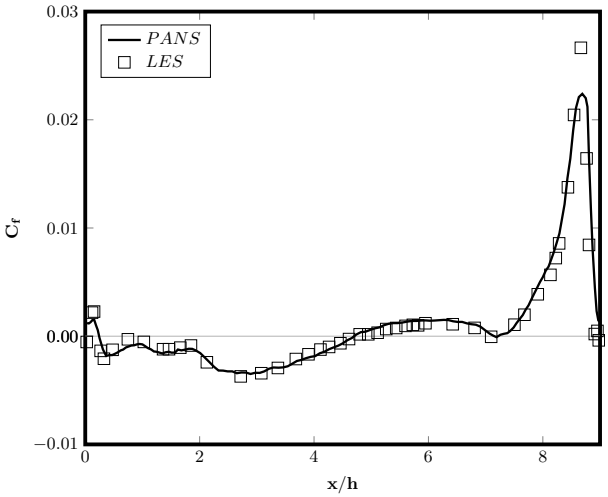

Figure 2: 2D hill's skin friction coefficient obtained by SSV-PANS in comparison with LES [20]

Table 1: Separation and reattachment points.

	LES[20]	PANS
x_s/h	0.22	0.24
x_r/h	4.72	4.70

0.21 ($C_\infty = 343$ m/s). For this Re and Ma number, the vortex shedding behind the cylinder radiates sound. The computational domain has a circular cross-section with a radius of $60D$ and span-wise length (L_s) of πD. Three different grids, with approximately 2.21, 4.42 and 9.55 million CVs are used. The reference LES results [1] are obtained with 17.7 million CVs. The inlet boundary condition is assumed as constant at the inlet ($U_0 = 72$ m/s). A pressure outlet boundary condition is assumed for the downstream boundary and a non-slip wall for the cylinder surface. As described in section 2.3, a two-dimensional acoustic field is used to compute the acoustic pressure in the mid-span plane of the hydrodynamic grid. Simulations are averaged for over 25 oscillation cycles after the oscillation behavior exhibits a quasi-periodic state. The acoustic pressure is extrapolated from the Kirchhoff surface (Located at a radius of 40D) to the observer's position in the far-field (Located at a radius of $185D$). Afterwards, using Equation 22, it is corrected from 2D to 3D. Figure 3 shows the pressure coefficient for different grids in comparison with the LES [14] and the experiments in [21]. The values agree well with the reference data. The distribution of f_k shown in Figure 4 demonstrates that f_k has smaller values when the grid is finer. The acoustic pressure shown in Figure 5 shows the dipole characteristics of the radiated sound which is because of vortex shedding at the back of the cylinder. Both in the LES [1] and the experiments [22], the corrected power spectrum density (PSD) are collected at an observer point, which is placed at a distance of $r = 185D$ from the cylinder's center perpendicular to the flow direction and are plotted in Figure 6. The results are compared in Table 2. The results correlate well with experimental data [22]. The broad peak

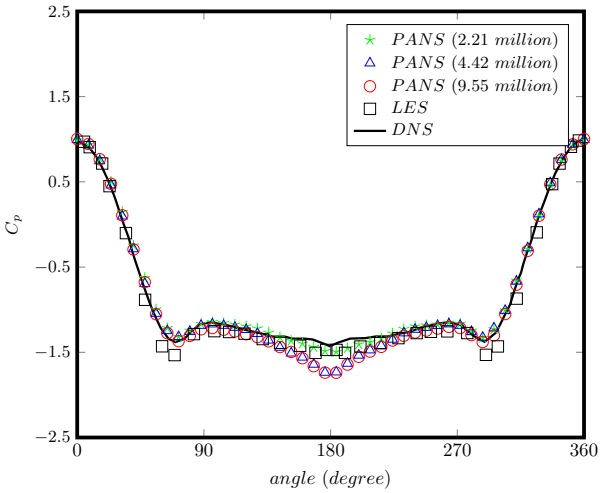

Figure 3: Cylinder's Pressure coefficient obtained by SSV-PANS in comparison with LES [14] and Experiment [21].

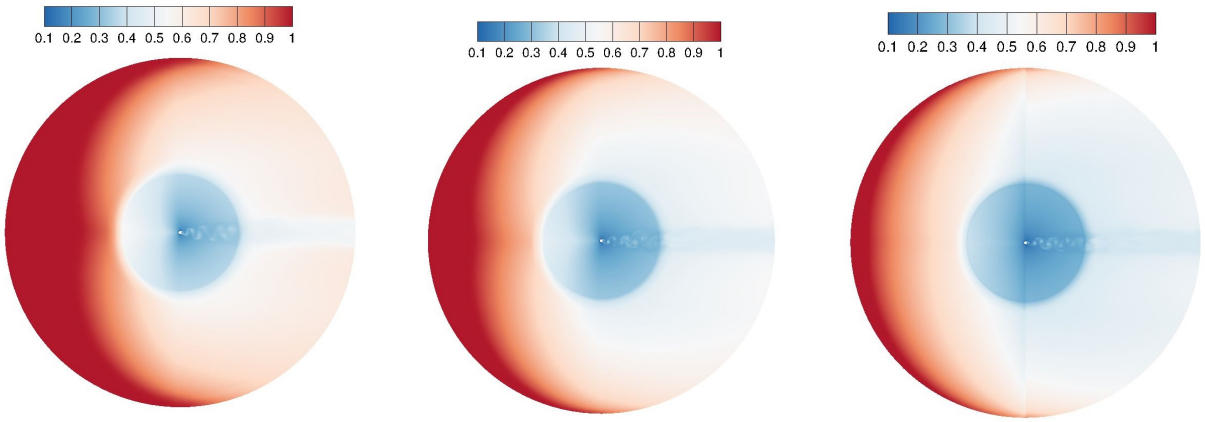

(a) 2.21 *million CVs* **(b)** 4.42 *million CVs* **(c)** 9.55 *million CVs*

Figure 4: Turbulent kinetic energy resolution parameter

which is located at the vortex shedding frequency is presented in Table 2 and is compared with the experimental data [1]. According to Figure 6 also the other two harmonics, which represent the lift and drag oscillations are present. However they can be better seen as the grids become finer. These results show that the aeroacoustic method based on the SSV-PANS method can predict broadband noise with reasonable accuracy. In addition, the computational efficiency of the SSV-PANS method for the calculation of the same amount of physical time is investigated for all the cases and are compared with LES with 17.7 million CVs under the same situation. The total time in terms of core hours, are presented in Table 2 for all the test cases. As it can be seen, the computational time decreases disproportionately with the number of CVs. The result depends on different parameters. First, the SSV-PANS model is based on the $k-\epsilon-\zeta-f$

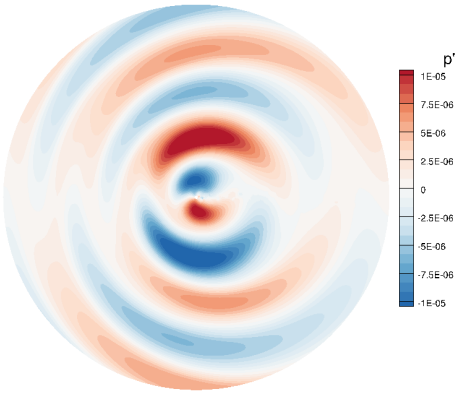

Figure 5: Acoustic pressure field of the cylinder.

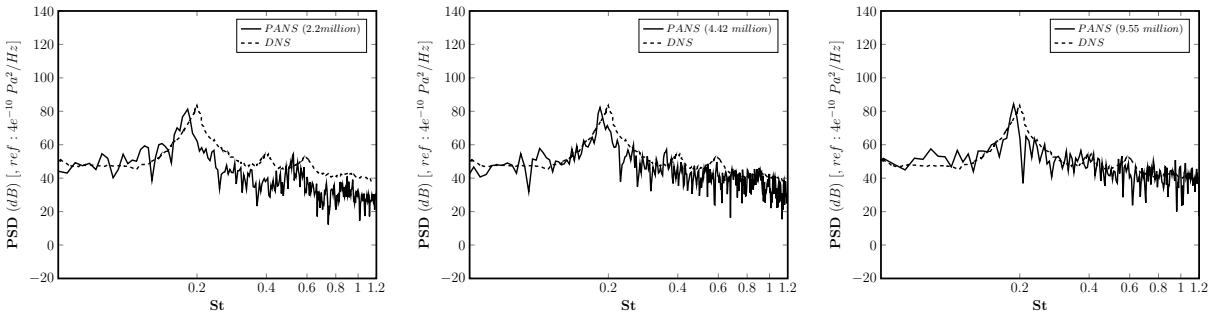

(a) 2.21 *million CVs* **(b)** 4.42 *million CVs* **(c)** 9.55 *million CVs*

Figure 6: Corrected power spectrum density (PSD) at an observer point.

Table 2: Comparison of the computational time and Strouhal frequency

	CVs (million)	Time ($core \times hour$)	CVs ratio -	Time ratio -	St -	Error (%)
PANS	2.21	110.8	0.13	0.07	0.182	8.5
PANS	4.42	377.5	0.25	0.25	0.184	7.5
PANS	9.55	1099.1	0.54	0.73	0.189	5.0
LES[1]	17.69	1508.8	1	1	0.195	2.0
Experiment[22]	-	-	-	-	0.199	-

equation, which solves two additional equations and causes extra computational time. On the other hand, the model uses the SSV equation, which causes a reduction in the computational time. Also, f_k depends on the grid size and has higher values for coarser grids, which means more modeled physics and less computational time. According to the above results, the aeroacoustic method based on the SSV-PANS is promising.

4 CONCLUSIONS

A hybrid computational aeroacoustic method has been used with three different grids to compute the sound generated around a cylinder with a subsonic Mach number. The validity of the SSV-PANS method has been shown using a periodic turbulent 2D-hill. The aeroacoustic computation has been based on an acoustic/viscous splitting technique with the SSV-PANS method to solve the incompressible flow field. A two-dimensional acoustic field is calculated on the mid-span plane with acoustic sources integrated into the span-wise direction. The incompressible field results agree well with LES and experimental data. The acoustic results show the method gives comparable results as LES and experiments with lower computational costs.

5 ACKNOWLEDGMENT

The work of Arezoo Moosavifard is supported by the Graduate School CE within the Centre for Computational Engineering at the Technical University of Darmstadt. All Calculations for this research have been conducted on the Lichtenberg high-performance computer of the TU Darmstadt. In addition, Arezoo Moosavifard is also grateful for the German Academic Exchange Service (DAAD) support through the Graduate School Scholarship Programme.

REFERENCES

[1] Kolb, E., and Schäfer, M. Aeroacoustic simulation of flexible structures in low Mach number turbulent flows. *Computers and Fluids.* (2021) **227**, 105020.

[2] Lighthill, M. J. On sound generated aerodynamically I. General theory. *Proceedings of the Royal Society of London. Series A. Mathematical and Physical Sciences.* (1952) **211**(1107), 564-587.

[3] Kornhaas, M., Schäfer, M., and Sternel, D. C. Efficient numerical simulation of aeroacoustics for low Mach number flows interacting with structures. *Computational Mechanics.* (2015) **55**(6), 1143–1154.

[4] Hardin, J. C., and Pope, D. S. An acoustic/viscous splitting technique for computational aeroacoustics. *Theoretical and computational fluid dynamics* (1994) **6**(5), 323–340.

[5] Reynolds, O. On the dynamical theory of incompressible viscous fluids and the determination of the criterion. *Philosophical transactions of the royal society of london. A.* (1895) **186**, 123-164.

[6] Smagorinsky, J. General circulation experiments with the primitive equations: I. The basic experiment. *Monthly weather review.* (1963) **91**(3), 99–164.

[7] Girimaji, S., Abdol-Hamid, K. S. Partially-averaged Navier-Stokes model for turbulence: Implementation and validation. *43rd AIAA Aerospace Sciences Meeting and Exhibit* (2005), p. 502.

[8] Girimaji, S. Partially-averaged Navier-Stokes model for turbulence: A Reynolds-averaged Navier-Stokes to direct numerical simulation bridging method. *Journal of Applied Mechanics.* (2006) **73**(3), 413–421.

[9] Abdol-Hamid, K. S., and Girimaji, S. A two-stage procedure toward the efficient implementation of PANS and other hybrid turbulence models. (2004).

[10] Huang, R., Luo, X., Ji, B., and Ji, Q. Turbulent flows over a backward facing step simulated using a modified partially averaged Navier–Stokes model. *Journal of Fluids Engineering.* (2017) **139**(4).

[11] Basara, B., Krajnovic, S., Girimaji, S., and Pavlovic, Z. Near-wall formulation of the Partially Averaged Navier Stokes turbulence model. *AIAA journal.* (2011) **49**(12), 2627–2636.

[12] Basara, B., Pavlovic, Z., and Girimaji, S. A new approach for the calculation of the cut-off resolution parameter in bridging methods for turbulent flow simulation. *International Journal of Heat and Fluid Flow.* (2018) **74**, 76–88.

[13] Fachgebiet für Numerische Berechnungsverfahren im Maschinenbau. FASTEST-Manual. *Technische Universität Darmstadt.* (2005).

[14] Seo, J. H., and Moon, Y. J. Aerodynamic noise prediction for long-span bodies. *Journal of Sound and Vibration.* (2018) **306**(3-5), 564–579.

[15] Gloerfelt, X., Bailly, C., and Juvé, D. Direct computation of the noise radiated by a subsonic cavity flow and application of integral methods. *Journal of sound and vibration.* (2003) **266**(1), 119–146.

[16] Girimaji, S., Srinivasan, R., and Jeong, E. PANS Turbulence Model for Seamless Transition Between RANS and LES: Fixed-Point Analysis and Preliminary Results. *Fluids Engineering Division Summer Meeting.* (2003) **36975**, 1901-1909.

[17] Durbin, P. A. Near-wall turbulence closure modeling without "damping functions". *Theoretical and computational fluid dynamics.* (1991) **3**(1), 1–13.

[18] Girimaji, S., and Basara, B. Modelling the cut-off scale supplying variable in bridging methods for turbulence flow simulation *Proc. of 4th Int. Conference on Jets, Wakes and Separated Flows.* (2013).

[19] Oberai, A. A., Roknaldin, F., and Hughes, T. J. Computation of trailing-edge noise due to turbulent flow over an airfoil. *AIAA journal.* (2002) **40**(11), 2206–2216.

[20] Fröhlich, J., Mellen, C. P., Rodi, W., Temmerman, L., and Leschziner, M. A. Highly resolved large-eddy simulation of separated flow in a channel with streamwise periodic constrictions. *Journal of Fluid Mechanics.* (2005) **526**, 19–66.

[21] Szepessy, S., and Bearman, P. W. Aspect ratio and end plate effects on vortex shedding from a circular cylinder. *Journal of Fluid Mechanics.* (1992) **234**, 191–217.

[22] Jacob, M. C., Boudet, J., Casalino, D., and Michard, M. A rod-airfoil experiment as a benchmark for broadband noise modeling. *Theoretical and Computational Fluid Dynamics.* (2005) **19**(3), 171–196.